Materials Research Bulletin 45 (2010) 1685–1691

Contents lists available at ScienceDirect

Materials Research Bulletin

journal homepage: www.elsevier.com/locate/matresbu

Rapid synthesis of room temperature ferromagnetic Ag-doped $LaMnO_3$ perovskite phases by the solution combustion method

Manjunath B. Bellakki [a], C. Shivakumara [a,*], N.Y. Vasanthacharya [a], A.S. Prakash [b]

[a] Solid State and Structural Chemistry Unit, Indian Institute of Science, Bangalore 560 012, India
[b] Central Electrochemical Research Institute-Chennai Unit, CSIR-Madras Complex, Chennai 600 113, India

ARTICLE INFO

Article history:
Received 18 December 2009
Received in revised form 28 June 2010
Accepted 29 June 2010
Available online 6 July 2010

Dedicated to Professor M.S. Hegde on the occasion of his 65th birthday.

Keywords:
A. Oxides
C. X-ray diffraction
D. Crystal structure
D. Magnetic properties

ABSTRACT

We report the rapid solution combustion synthesis and characterization of Ag-substituted $LaMnO_3$ phases at relatively low temperature using oxalyl dihydrazide, as fuel. Structural parameters were refined by the Rietveld method using powder X-ray diffraction data. While the parent $LaMnO_3$ crystallizes in the orthorhombic structure, the Ag-substituted compounds crystallize in the rhombohedral symmetry. On increasing Ag-content, unit cell volume and Mn–O–Mn bond angle decreases. The Fourier transform infra red spectrum shows two absorption bands corresponding to Mn–O stretching vibration (ν_s mode) and Mn–O–Mn deformation vibration (ν_b mode) around 600 cm^{-1} and 400 cm^{-1} for the compositions, $x = 0.0$, 0.05 and 0.10, respectively. Electrical resistivity measurements reveal that composition-controlled metal to insulator transition, with the maximum metal to insulator being 280 K for the composition $La_{0.75}Ag_{0.25}MnO_3$. Increase in magnetic moment was observed with increase in Ag-content. The maximum magnetic moment of 35 emu/g was observed for the composition $La_{0.80}Ag_{0.20}MnO_3$.

1. Introduction

Divalent ion-doped rare-earth manganites of the general formula $Ln_{1-x}A_xMnO_3$ (Ln = rare-earth ion and A = Ca, Sr, Ba and Pb) are a subject of interest due to their interesting properties such as insulator-to-metal (I–M) transition, charge, spin, orbital ordering, and colossal magnetoresistance [1–3]. The ratio of Mn^{3+}/Mn^{4+} is an important factor to show insulator-to-metal (I–M) transition and magnetic phase transition in manganites. Generally, divalent ion-doped manganites exhibit composition-controlled I–M transition. It is possible to achieve an equal amount of hole doping with just half the quantity of monovalent ions, because for the same amount of aliovalent dopant the hole density is twice that of the divalent ion doping. Monovalent ions like alkali metal ion-doped rare-earth manganites of the general formula $Ln_{1-x}A_xMnO_3$ (Ln = La, Pr, Nd; A = Ag, K, Rb) provide a series of new oxides to study the physical phenomena of insulator-to-metal transition and colossal magnetoresistance [4–9]. Recently there have been few reports on Ag^+-substituted $LaMnO_3$, another series of novel oxides which exhibit ferromagnetic metal to paramagnetic insulators (FMM–PI) transition with high CMR effect at room temperature. These compounds were synthesized by conventional solid state methods [10–13], pyrophoric method [14] and sol gel method [15]. These methods require high temperature (1000–1250 °C) and heating times of 48 h. Gorbenko et al. [16] reported that the vacancies in the A-sublattice of the perovskite structure $La_{1-x}MnO_{3+\delta}$ can be filled by Ag^+ ions under the soft conditions of synthesis. Recently, Melnikov et al. [17] showed Ag-doped manganite nanoparticles are new materials for temperature controlled medical hyperthermia.

The solution combustion method offers an advantage over the other conventional methods in that it is a low-temperature initiated exothermic and self-propagating process. Patil et al. [18] have reviewed the synthesis of various oxide materials by the combustion reactions of redox mixtures containing stoichiometric amount of respective metal nitrates (oxidizers) and fuels such as urea, hydrazides (Carbohydrazide, CH), oxalyldihydrazide (ODH), malonic acid dihydrazide (MDH), tetraformaltrisazine (TFTA) and glycine. Using the solution combustion method, a wide range of technologically useful oxides having magnetic, dielectric, electrical, mechanical, luminescent and optical properties were prepared. Bera et al. synthesized new redox catalysts of Ag/CeO_2 [19] and Cu/CeO_2 [20]. This method was also applied to prepare divalent ion-doped lanthanum manganites [21]. Nanocrystalline $La_{1-x}Ba_xMnO_3$ [22], $La_{1-x}Sr_xMnO_3$ [23] and sodium-doped lanthanum manganites have been prepared by the sol gel, propellant and combustion

* Corresponding author. Tel.: +91 80 2293 2951; fax: +91 80 2360 1310.
E-mail address: shiva@sscu.iisc.ernet.in (C. Shivakumara).

0025-5408/$ – see front matter © 2010 Elsevier Ltd. All rights reserved.
doi:10.1016/j.materresbull.2010.06.063

method [24,25]. Recently, Shivakumara et al. [26], have reported the ferromagnetic and metallic $La_{1-x}K_xMnO_3$ $(0.0 \le x \le 0.25)$ phases. In the present work we report for the first time, rapid synthesis of room temperature ferromagnetic and metallic oxides of silver substituted lanthanum manganites phases by the solution combustion method at a relatively low temperature and a shorter duration of 2 h.

2. Experimental

The powder samples of $La_{1-x}Ag_xMnO_3$ $(0.00 \le x \le 0.25)$ were prepared by the solution combustion method using oxalyl dihydrazide (ODH) as a fuel. The detailed procedure for calculating the metal nitrates to fuel ratio has been described elsewhere [18,27]. In a typical preparation of $La_{0.85}Ag_{0.15}MnO_3$ compound, preheated (800 °C) lanthanum oxide, La_2O_3 (1.3847 g) was dissolved in 10 ml of 8 M nitric acid, HNO_3, silver nitrate, $AgNO_3$ (0.2518 g) and manganese nitrate, $Mn(NO_3)\cdot 4H_2O$ (2.5101 g) were dissolved in 20 ml of deionized water. Both the solutions were mixed in a Pyrex dish of dimension 100 mm × 50 mm and the fuel oxalyldihydrazide (ODH), $C_2H_2N_4O_2$ (1.1814 g) was added. The reaction mixture was heated on a hot plate at 80 °C to obtain a clear solution. Finally, the Pyrex dish containing the reaction mixture was introduced into a muffle furnace (dimension 15 cm × 15 cm × 30 cm) preheated to 400 °C. The reaction mixture was boiled, followed by frothing and then ignited with evolution of large amounts of gases. The flame persisted for about a minute, leaving behind a residual black colored fine powder. Assuming complete combustion, the general equation for the formation of samples can be proposed as follows:

$$(1-x)La(NO_3)_3(aq) + xAg(NO_3)(aq) + Mn(NO_3)_2(aq) + C_2H_6N_4O_2(aq) \rightarrow La_{1-x}Ag_xMnO_3(S) + CO_2(g) + H_2O(g) + N_2(g)$$

The resulting powders were X-ray amorphous in nature. To obtain crystallininty, the powders were heated at 800 °C with varying time from 5 min to 2 h, phase evolution was also monitored at different temperatures (500–800 °C) at constant time (1 h). All the samples were characterized by powder X-ray diffraction (XRD) using a Philips Xpert Pro diffractometer with Cu Kα (λ = 1.5418 Å) radiation using a graphite monochromator. For Rietveld refinement, Data were collected at a scan rate of 1°/min. with a 0.02° step size for 2θ from 10° to 80°. The data were refined using the FullProf Suite-2000 version. Infrared spectra of calcined samples were recorded on a Perkin-Elmer FT-IR Spectrometer Spectrum 1000 in the range of 300–4000 cm^{-1}. Electrical resistivity measurements were carried out on sintered pellets (800 °C, 12 h) by the four-probe method in the temperature range from 300 to 12 K. Room temperature magnetic measurements were carried out using vibrating sample a magnetometer (VSM), Lake Shore.

3. Results and discussions

The exothermicity of the combustion reaction depends on the oxidizer (O) to fuel (F) ratio and the maximum exothermicity is observed when O/F = 1. In the present study, we have controlled the exothermicity of the reaction by making it fuel-lean by adding excess nitrate source (Oxidizer). It is necessary to moderate the flame temperature (exothermicity) in order to suppress the reduction of Ag^+ ion to Ag^0 metal during combustion process. As a result of lower exothermicity the products formed were amorphous. Fig. 1, shows the powder X-ray diffraction patterns of the typical $La_{0.85}Ag_{0.15}MnO_3$ as-synthesized and of sintered samples at 800 °C for varying duration of 5 min to 2 h. The as-synthesized compound is amorphous in nature. However a crystalline perovskite phase was formed within 5 min of sintering at 800 °C. The indexed

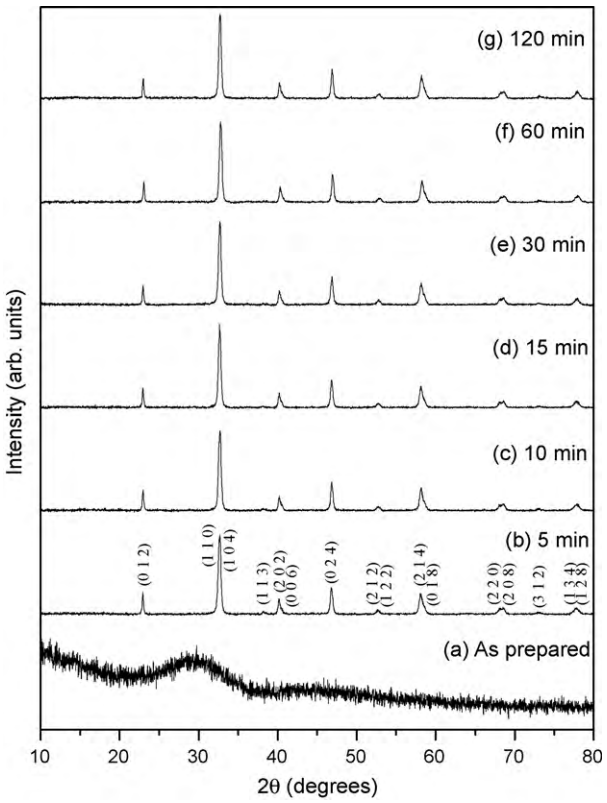

Fig. 1. Powder X-ray diffraction patterns of $La_{0.85}Ag_{0.15}MnO_3$ (a) as-prepared and (b–g) calcined at 800 °C from 5 min to 2 h.

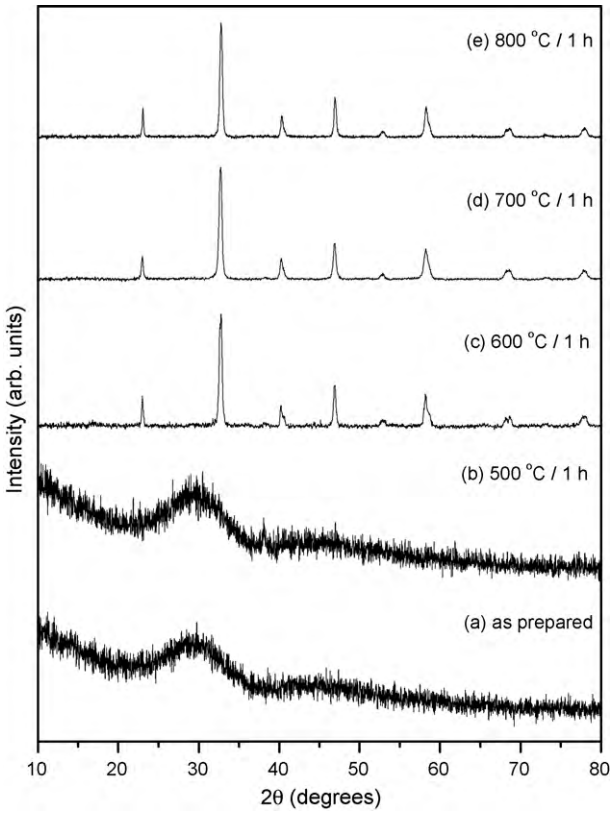

Fig. 2. (a–e) Powder X-ray diffraction patterns of $La_{0.85}Ag_{0.15}MnO_3$ compound calcined at different temperature from 500 to 800 °C/1 h.

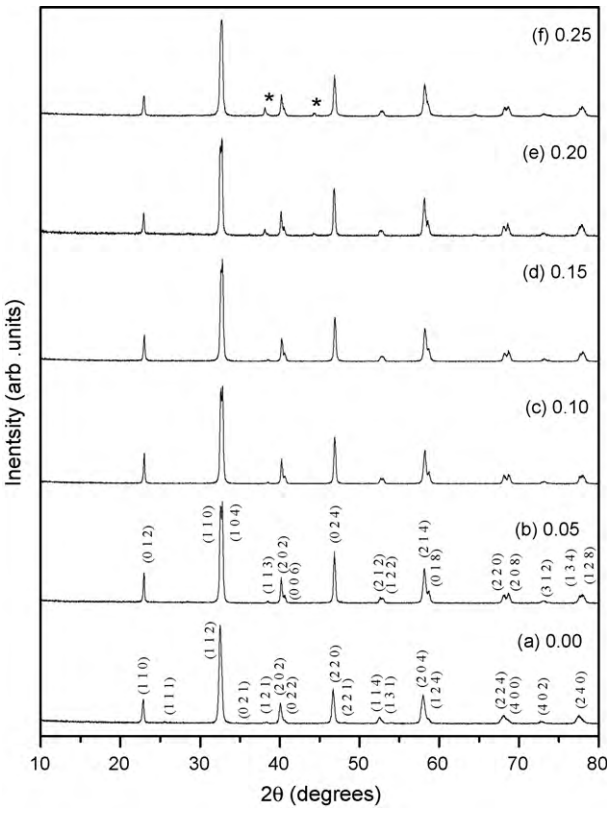

Fig. 3. (a–f) Powder X-ray diffraction patterns of $La_{1-x}Ag_xMnO_3$ ($0.00 \le x \le 0.25$) phases, calcined at 800 °C/12 h (asterisk indicates Ag metal impurity peaks).

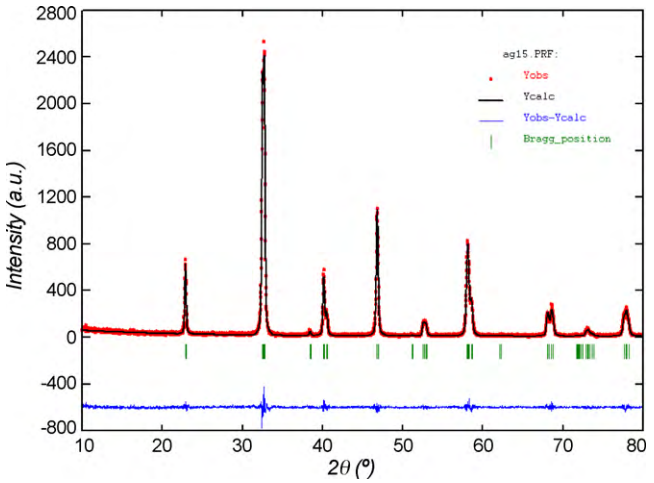

Fig. 4. Typical observed, calculated and the difference Rietveld refined X-ray diffraction patterns of $La_{0.85}Ag_{0.15}MnO_3$.

powder XRD pattern of the sample sintered for 5 min is shown in Fig. 1(b). All the diffracted lines are indexed in space group $R\bar{3}c$ (hexagonal setting) with lattice parameters $a = 5.504(5)$ Å and $c = 13.349(8)$ Å. There were no structural changes with increasing sintering time. The average crystallite size for $La_{0.85}Ag_{0.15}MnO_3$ from XRD data, calculated using the Scherrer formula [28], was found to be in the range of 30–33 nm. No significant changes were observed in crystallite size when the sintering times were increased from 5 min to 2 h. Study of the phase evolution by varying the sintering temperature from 500 to 800 °C at a fixed duration of an hour (Fig. 2), reveals that crystallization is induced at 600 °C. Further, there were no structural changes with increase in sintering temperatures.

Fig. 3 shows the powder XRD patterns of $La_{1-x}Ag_xMnO_3$ ($0.00 \le x \le 0.25$) compounds sintered at 800 °C for 12 h. The parent $LaMnO_3$ compound crystallizes in the orthorhombic structure with space group *Pbnm* (No. 62), and the indexed diffraction pattern is shown in Fig. 3(a). The Ag-substituted compounds crystallize in the rhombohedral structure (hexagonal setting) with space group $R\bar{3}c$ (No. 167) and the indexed powder XRD pattern is given for $La_{0.95}Ag_{0.05}MnO_3$ in Fig. 3(b). At $x = 0.25$, we do observe a small amount (~5%) of Ag metal as an impurity phase. As the silver content was increased from $x = 0.05$ to 0.25, the rhombohedral phase transforms to cubic-like symmetry (Fig. 3(b)–(f)). The splitting of the main (1 1 0) and (1 0 4) lines decrease and seems to merge into one line with increasing Ag-content. The structural parameters for all the phases were obtained from the Rietveld refinement method. The refinement result reveals that even the composition $x = 0.25$ crystallizes in the rhombohedral structure with a lower rhombohedral distortion. The observed, calculated and the difference XRD pattern of the typical $La_{0.85}Ag_{0.15}MnO_3$ compound is given in Fig. 4. There is a good agreement between observed and calculated patterns. In Table 1, we have summarized refined structural parameters, Mn–O bond lengths and Mn–O–Mn bond angles for all the samples. Variation of the lattice parameters as a function of average A-site cation radius $\langle r_A \rangle$ is given in Fig. 5. As '*a*' parameter increases, '*c*' parameter decreases with increase in average $\langle r_A \rangle$. In Fig. 6, we have shown the plots of (a) unit cell volume per formula unit and (b) Mn–O–Mn bond angle as a function of Ag-content. When Ag-content increases from $x = 0.05$ to 0.25, the unit cell volume decreases from 58.45 to 58.33 Å^3 and Mn–O–Mn bond angle decreases from 164.80° to 161.95°. The decreases in cell volumes and Mn–O–Mn bond angles can be correlated with the smaller size of the average A-site cation ($r_{La^{3+}} = 1.36$ Å; $r_{Ag^{+}} = 1.28$ Å) and also the decrease in average size of the B-site cation due to increase in Mn^{4+} content, which is smaller ($r_{Mn^{4+}} = 0.53$ Å) than Mn^{3+} ion ($r_{Mn^{3+}} = 0.645$ Å) [29]. A similar observation was found by Dhahri et al. [30] in $La_{1-x}Cd_xMnO_3$ ($0.1 \le x \le 0.5$) system.

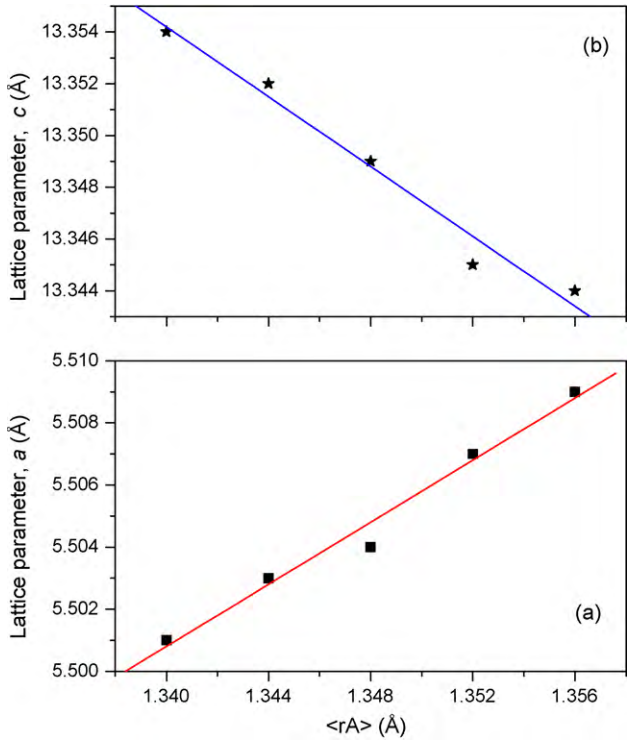

Fig. 5. (a and b) Variation of the lattice parameters as a function of average A-site cation radius $\langle r_A \rangle$ in $La_{1-x}Ag_xMnO_3$ ($0.00 \le x \le 0.25$).

Table 1
Rietveld refined structural parameters, selected bond lengths and bond angles of $La_{1-x}Ag_xMnO_3$ compounds.

Compounds	$LaMnO_3$	$La_{0.95}Ag_{0.05}MnO_3$	$La_{0.90}Ag_{0.10}MnO_3$	$La_{0.85}Ag_{0.15}MnO_3$	$La_{0.80}Ag_{0.20}MnO_3$	$La_{0.75}Ag_{0.25}MnO_3$
Crystal system space group	Orthorhombic, *Pbnm* (62)	Rhombohedral, $R\bar{3}c$ (167)	Rhombohedral, $R\bar{3}c$ (167)	Rhombohedral, $R\bar{3}c$ (167)	Rhombohedral, $R\bar{3}c$ (167)	Rhombohedral, $R\bar{3}c$ (167)
Lattice parameters						
a (Å)	5.477(6)	5.509(5)	5.507(7)	5.504(5)	5.503(7)	5.501(8)
b (Å)	5.524(4)					
c (Å)	7.805(6)	13.344(6)	13.345(4)	13.349(8)	13.352(8)	13.354(9)
Cell volume/formula unit (Å^3)	59.05(1)	58.45(4)	58.43(4)	58.37(3)	58.36(2)	58.33(7)
Distortion, α (°)		60.49	60.47	60.43	60.42	60.39
La/Ag	(4e)	(6a)	(6a)	(6a)	(6a)	(6a)
x	0.005(12)	0.0000	0.0000	0.0000	0.0000	0.0000
y	0.0120(5)	0.0000	0.0000	0.0000	0.0000	0.0000
z	0.2500	0.2500	0.2500	0.2500	0.2500	0.2500
Mn	(4b)	(6b)	(6b)	(6b)	(6b)	(6b)
x	0.5000	0.0000	0.0000	0.0000	0.0000	0.0000
y	0.0000	0.0000	0.0000	0.0000	0.0000	0.0000
z	0.0000	0.0000	0.0000	0.0000	0.0000	0.0000
O1	(4e)	(18e)	(18e)	(18e)	(18e)	(18e)
x	0.0109(7)	0.453(8)	0.452(4)	0.449(6)	0.449(7)	0.444(2)
y	0.4869(6)	0.0000	0.0000	0.0000	0.0000	0.0000
z	0.2500	0.2500	0.2500	0.2500	0.2500	0.2500
O2	(8d)					
x	0.7500(8)					
y	0.2803(6)					
z	0.0675(3)					
R-factors						
R_P	0.123	0.076	0.067	0.067	0.093	0.095
R_{WP}	0.180	0.119	0.112	0.114	0.148	0.174
R_{Bragg}	0.048	0.025	0.015	0.015	0.031	0.037
R_F	0.046	0.020	0.014	0.013	0.027	0.034
Bond lengths and angles						
Mn–O1–Mn (°)	174.49(5)	164.80(4)	164.48(7)	163.53(5)	163.53(2)	161.95(3)
Mn–O2–Mn (°)	148.86(8)					
Mn–O1 (Å)	1.953(7)	1.958(2)	1.958(5)	1.960(8)	1.961(3)	1.963(9)
Mn–O2 (Å)	2.133(2)					
Mn–O2′ (Å)	1.904(2)					

FT-IR spectra of $La_{1-x}Ag_xMnO_3$ ($0.00 \le x \le 0.25$) compounds are shown in Fig. 7. The IR spectra show two absorption bands around 600 and 400 cm^{-1} for the compositions: (a) $x = 0.0$, (b) 0.05 and (c) 0.10. The higher frequency band at 600 cm^{-1} was assigned to the Mn–O stretching vibration (ν_s) mode, which involves the internal motion of a change in Mn–O bond length and the band around 400 cm^{-1} corresponds to the bending mode (ν_b), which is sensitive to a change in the Mn–O–Mn bond angle. These two bands are related to the environment surrounding the MnO_6 octahedra in the ABO_3 perovskite [31,32]. These absorptions bands disappear in metallic compounds due to lack of static dipole. In $La_{1-x}Ag_xMnO_3$, when *x* exceeds 0.15, on account of the metallic nature of the compound absorption bands disappear.

In Fig. 8, are shown the plots of resistivity as a function of temperature for $La_{1-x}Ag_xMnO_3$ ($0.00 \le x \le 0.25$) pellets sintered at 800 °C for 12 h. The composition $x = 0.00$, exhibits insulating behavior. With increase in silver content, a composition-controlled metal to insulator transition (T_{M-I}) was observed. The T_{M-I} values obtained are 120, 200, 254, 275 and 280 K for the compositions $x = 0.05$, 0.10, 0.15, 0.20 and 0.25, respectively. Generally, solid state preparations give bigger grain size and exhibit sharp metal insulator transitions. However, in the present study, all the samples show a broad metal insulator transition, which we attribute to the nanocrystalline nature of the grains and weak grain boundary contact. The effect of grain size on magnetic, transport and structural properties of manganites have been extensively studied by many investigators [33–36]. These studies suggest that particle size, the doping level in the lanthanum site as well as oxygen content play an important role in the above properties of these classes of oxides.

Phase evolution as a function of time and temperature was correlated with magnetic properties. We have performed the room temperature VSM measurements for $La_{0.85}Ag_{0.15}MnO_3$ system. In Fig. 9(a)–(g), we have shown the magnetic moment as a function of applied field for $La_{0.85}Ag_{0.15}MnO_3$ compound sintered at 800 °C from 5 min to 2 h. The as-prepared compound did not show any magnetization, due to the amorphous in nature of the compound. On increasing sintering time from 5 min to 2 h, the magnetic moment increased with increased calcination time. The maximum moment of 33 emu/g was observed for the compound calcined at 800 °C/2 h.

Similarly, we carried out the magnetization measurement for $La_{0.85}Ag_{0.15}MnO_3$ calcined at different temperature from 500 to 800 °C for fixed duration of 1 h, as shown in Fig. 10(a)–(e). From Fig. 10 it is clear that the samples calcined up to 600 °C for 1 h did not show any magnetization up to 10 kOe. Further, the samples calcined at 700 and 800 °C showed magnetic moments of 20 and 31 emu/g, respectively. Fig. 11 shows the variation in magnetic moment as a function of (a) calcination time, (b) calcination temperature and (c) Ag-content. It is evident that the magnetic

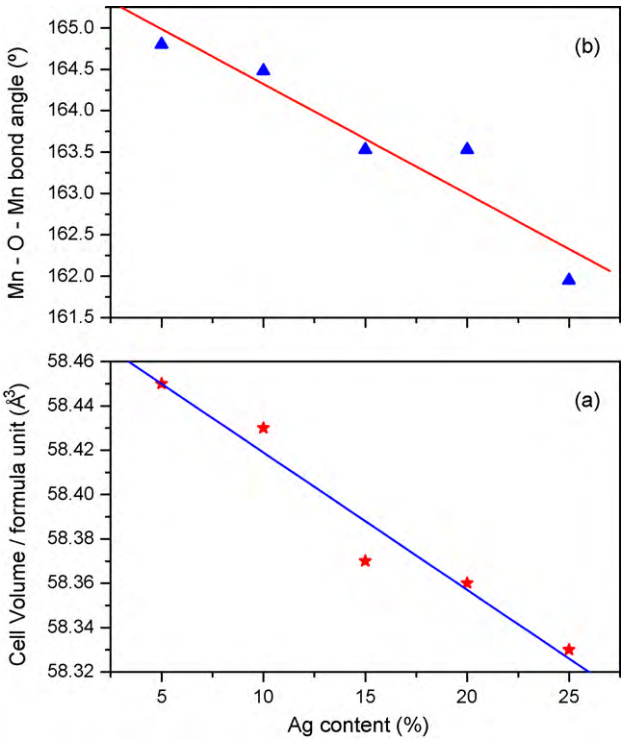

Fig. 6. Plots of (a) unit cell volume per formula unit and (b) Mn–O–Mn bond angle as a function of Ag ion content in $La_{1-x}Ag_xMnO_3$.

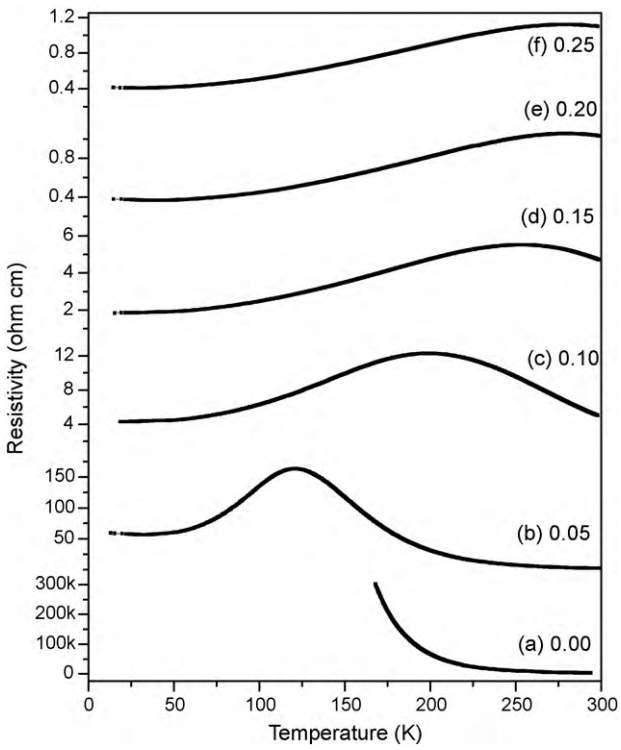

Fig. 8. (a–f) Plot of electrical resistivity as a function of temperature for $La_{1-x}Ag_xMnO_3$ ($0.00 \leq x \leq 0.25$), pellets sintered at 800 °C/12 h.

moment increased with increasing calcination temperature up to 30 min, but on further heating there was not much change in magnetic moment. Fig. 11(b), reveals that as-synthesized and 500 °C heated samples did not show any magnetization, due to the amorphous nature of the samples. Although a crystalline single phase perovskite was observed at 600 °C, no magnetization was seen up to 10 kOe. Samples sintered at 700 °C and above, crystallized in the rhombohedral structure and exhibited magnetic moments of 20 and 31 emu/g, respectively. These results clearly demonstrate that structural ordering precedes magnetic ordering and the sintering time and temperature play a critical role in the determining the magnetic property.

In Fig. 12, we have shown the magnetic moment as a function of applied field for all the compositions of $La_{1-x}Ag_xMnO_3$ MnO_3 ($0.00 \leq x \leq 0.25$) sintered at 800 °C for 12 h. The compositions (a) $x = 0.00$ and (b) 0.05 did not show any ferromagnetic ordering up to 10 kOe. On the other hand, as the silver content

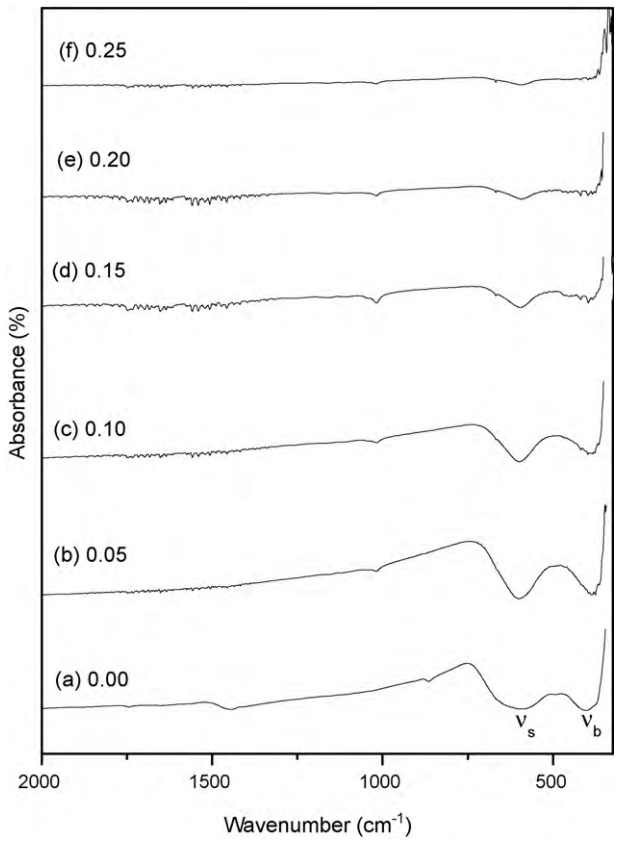

Fig. 7. (a–f) FT-IR spectra of $La_{1-x}Ag_xMnO_3$ ($0.00 \leq x \leq 0.25$) phases.

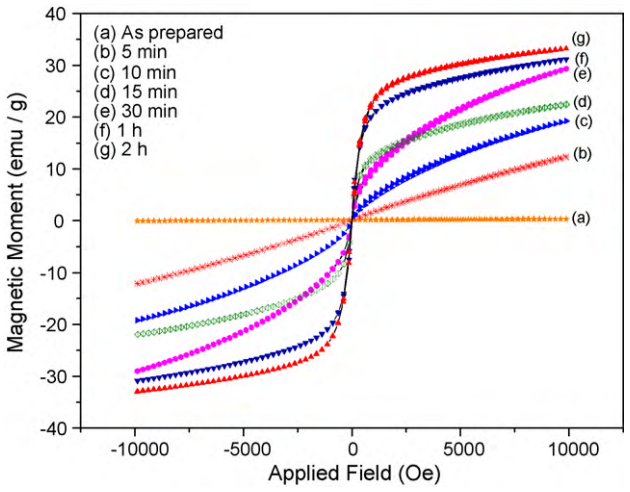

Fig. 9. (a–g) Plot of magnetic moment as a function of applied field for $La_{0.85}Ag_{0.15}MnO_3$ calcined at 800 °C from 5 min to 2 h.

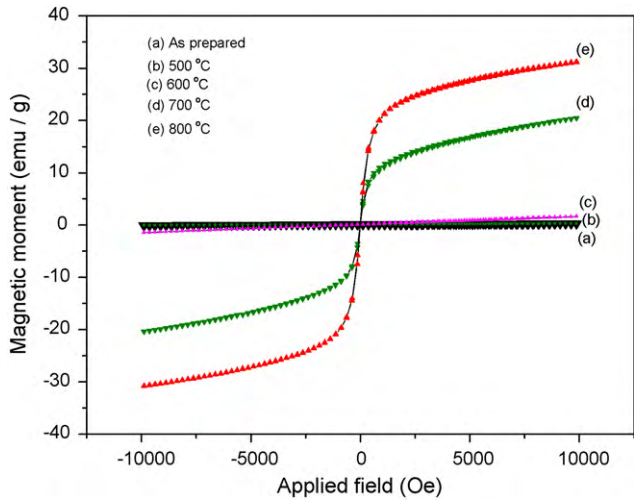

Fig. 10. (a–e) Plot of magnetic moment as a function of applied field for $La_{0.85}Ag_{0.15}MnO_3$ compounds calcined at different temperature from 500 to 800 °C/1 h.

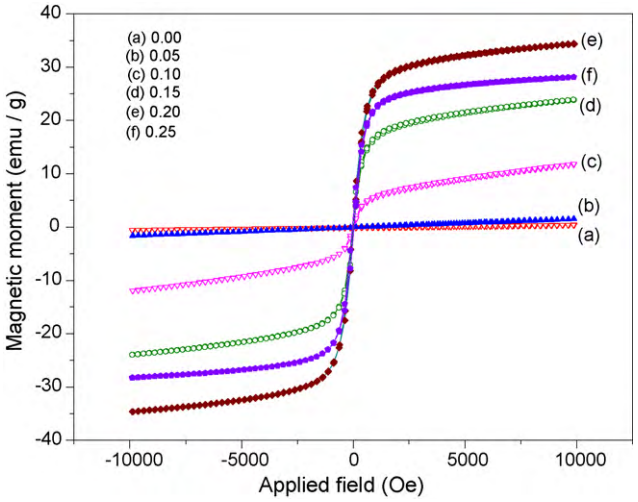

Fig. 12. (a–e) Plot of magnetic moment as a function of applied field for $La_{1-x}Ag_xMnO_3$ ($0.00 \le x \le 0.25$) compounds sintered at 800 °C for 12 h.

increased from (c) 0.10, (d) 0.15, (e) 0.20 and (f) 0.25 compounds exhibited ferromagnetic properties with magnetic moments of 12, 24, 35 and 28 emu/g, respectively. Magnetic moment of $La_{0.75}Ag_{0.25}MnO_3$ phase is lower than that of $La_{0.80}Ag_{0.20}MnO_3$ (Fig. 11(c)). This can be correlated with ratio of Mn^{3+}/Mn^{4+} ions. When La^{3+}-ions partially replaced by Ag^{+} ions in $LaMnO_3$ will produce more Mn^{4+} as well as a valence difference. This favors electronic inhomogeneity and induces possible phase or domain separation [37], which are due to formation of Mn^{4+} rich regions and Mn^{3+} rich regions. This electronic inhomogeneity produces antiferromagnetic insulating (AFI) phases, ferromagnetic insulating (FMI) phases and ferromagnetic metallic (FMM) phases [38]. In the present study $La_{0.75}Ag_{0.25}MnO_3$ system, concentration of Mn^{4+} ions are more compared to the $La_{0.80}Ag_{0.20}MnO_3$, which favors the antiferromagnetic interaction within the ferromagnetic clusters [39]. Washburn et al. [40], have analyzed such a magnetic behavior taking into account two lattice model; one with ferromagnetic interaction and the second with antiferromagnetic interaction. Here, in addition to the Mn^{3+}–O–Mn^{4+} double exchange interaction leading to ferromagnetic behavior, the Mn^{4+}–O–Mn^{4+} antiferromagnetic interaction is bringing down the ferromagnetic interaction and hence the magnetic moment is lower in $La_{0.75}Ag_{0.25}MnO_3$ system.

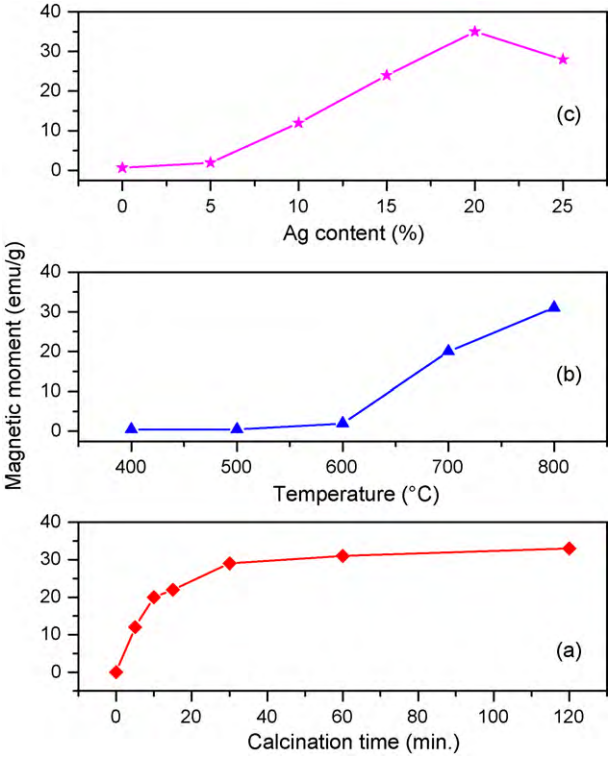

Fig. 11. Plots of magnetic moment as a function of (a) calcination time, (b) calcination temperature for $La_{0.85}Ag_{0.15}MnO_3$, and (c) magnetic moment as function of Ag-content in the $La_{1-x}Ag_xMnO_3$ system.

4. Conclusions

In conclusion, Ag-substituted lanthanum manganite perovskite phases are synthesized by the rapid solution combustion method at relatively low temperature. Structural transition was observed from orthorhombic to rombohedral upon Ag-substitution to La-site. We observed the structural ordering temperature as low as 500 °C and shorter duration of 5 min at 800 °C. XRD and VSM data reveal structural ordering precedes magnetic ordering. The sintering time and temperature play an important role in determining the magnetic ordering.

Acknowledgements

We thank Department of Science and Technology (FIST - DST), Government of India, New Delhi for providing XRD, VSM facilities. We also extend our thanks to Mr. I.S. Jarali for his help in recording FT-IR spectra. Special thanks are due to Professor M.S. Hegde, SSCU, Indian Institute of Science for useful discussion.

References

[1] G.H. Jonker, J.H. van Santen, Physica 16 (1950) 337.
[2] C.N.R. Rao, A.K. Cheetham, R. Mahesh, Chem. Mater. 8 (1996) 2421.
[3] C.N.R. Rao, J. Phys. Chem. B104 (2000) 5877.
[4] M. Itoh, T. Shimura, J.D. Yu, T. Hayashi, Y. Inaguma, Phys. Rev. B52 (1995) 12522.
[5] T. Shimura, T. Hayashi, Y. Inaguma, M. Itoh, J. Solid State Chem. 124 (1996) 250.
[6] M. Sahana, R.N. Singh, C. Shivakumara, N.Y. Vasanthacharya, M.S. Hegde, S. Subramanian, V. Prasad, S.V. Subramanyam, Appl. Phys. Lett. 70 (1997) 2909.
[7] C.C. Chen, A. de Lozanne, Appl. Phys. Lett. 71 (1997) 1424.
[8] Y. Ng-Lee, F. Safina, E. Martinez-Tamayo, J.V. Folgado, R. Ibanez, D. Beltran, F. Lloret, A. Segura, J. Mater. Chem. 7 (1997) 1905.

[9] R.N. Singh, C. Shivakumara, N.Y. Vasanthacharya, S. Subramanian, M.S. Hegde, S. Rajagopal, A. Sequeira, J. Solid State Chem. 137 (1998) 19.
[10] T. Tang, K.M. Gu, Q.Q. Cao, D.H. Wang, S.Y. Zhang, Y.W. Du, J. Magn. Magn. Mater. 222 (2000) 110.
[11] N.T. Hien, N.P. Thuy, Physica B 319 (2002) 168.
[12] L. Pi, M. Hervieu, A. Maignan, C. Martin, B. Raveau, Solid State Commun. 126 (2003) 229.
[13] T. Tao, Q.Q. Cao, K.M. Gu, H.Y. Xu, S.Y. Zhang, Y.W. Du, Appl. Phys. Lett. 77 (2000) 723.
[14] M. Battabyal, T.K. Dey, Solid State Commun. 131 (2004) 337.
[15] W. Ke, N. Zhang, T. Geng, R. Gao, J. Magn. Magn. Mater. 312 (2007) 430.
[16] O.Yu. Gorbenko, O.V. Melnikov, A.R. Kaul, A.M. Balagurov, S.N. Bushmeleva, L.I. Koroleva, R.V. Demin, Mater. Sci. Eng. B 116 (2005) 64.
[17] O.V. Melnikov, O.Yu. Gorbenko, M.N. Markelova, A.R. Kaul, V.A. Atsarkin, V.V. Demidov, C. Soto, E.J. Roy, B.M. Odintsov, J. Biomed. Mater. Res. Part A 91 (2009) 1048.
[18] K.C. Patil, S.T. Aruna, S. Ekambaram, Curr. Opin. Solid State Mater. Sci. 2 (1997) 158.
[19] P. Bera, K.C. Patil, M.S. Hegde, Phys. Chem. Chem. Phys. 2 (2000) 3715.
[20] P. Bera, S.T. Aruna, K.C. Patil, M.S. Hegde, J. Catal. 186 (1999) 36.
[21] S.T. Aruna, M. Muthuraman, K.C. Patil, J. Mater. Chem. 7 (1997) 2499.
[22] B.M. Nagabhushana, G.T. Chandrappa, R.P. Sreekanth Chakradhar, K.P. Ramesh, C. Shivakumara, Solid State Commun. 136 (2005) 427.
[23] B.M. Nagabhushana, R.P. Sreekanth Chakradhar, K.P. Ramesh, C. Shivakumara, G.T. Chandrappa, Mater. Res. Bull. 41 (2006) 1735.
[24] L. Malavasi, M.C. Mozzati, S. Polizzi, C.B. Azzoni, G. Flor, Chem. Mater. 15 (2003) 5036.
[25] C. Shivakumara, M.B. Bellakki, A.S. Prakash, N.Y. Vasanthacharya, J. Am. Ceram. Soc. 90 (2007) 3852.
[26] C. Shivakumara, M.B. Bellakki, Bull. Mater. Sci. 32 (2009) 443.
[27] K.C. Patil, Bull. Mater. Sci. 16 (1993) 533.
[28] Scherrer, Nachr. Ges. Wiss. Gottingen, Math.-Phys. 2 (1918) 98.
[29] R.D. Shannon, Acta Cryst. A 32 (1976) 751.
[30] A. Dhahri, J. Dhahri, S. Zemni, M. Oumezzine, M. Said, H. Vincent, J. Alloys Compd. 450 (2008) 12.
[31] F. Gao, R.A. Lewis, X.L. Wang, S.X. Dou, J. Alloys Compd. 347 (2002) 314.
[32] A. Arulraj, C.N.R. Rao, J. Solid State Chem. 145 (1999) 557.
[33] R. Mahendiran, R. Mahesh, A.K. Raychaudhuri, C.N.R. Rao, Solid State Commun. 99 (1996) 149.
[34] J. Wang, B. Gu, H. Sang, G. Ni, Y. Du, J. Magn. Magn. Mater. 223 (2001) 50.
[35] J. Yang, B.C. Zhao, R.L. Zhang, Y.Q. Ma, Z.G. Sheng, W.H. Song, Y.P. Sun, Solid State Commun. 132 (2004) 83.
[36] L.E. Hueso, F. Rivadulla, R.D. Sanchez, D. Caeiro, C. Jardon, C. Vazquez-Vazquez, J. Rivas, M.A. Lopez-Quintela, J. Magn. Magn. Mater. 189 (1998) 321.
[37] S.L. Ye, W.H. Song, J.M. Dai, S.G. Wang, K.Y. Wang, C.L. Yuan, Y.P. Sun, J. Appl. Phys. 88 (2000) 5915.
[38] G.N. Rao, S. Roy, R.C. Yang, J.W. Chen, J. Magn. Magn. Mater. 260 (2003) 375.
[39] C. Shivakumara, G.N. Subbanna, N.P. Lalla, M.S. Hegde, Mater. Res. Bull. 39 (2004) 71.
[40] N.R. Washburn, A.M. Stacy, J. Phys. Chem. B 104 (2000) 1447.